# Hydrodynamic coefficients of a simplified floating system of gravity cage in waves[*]

Chang-wen WU[1], Fu-kun GUI[†‡1,3], Yu-cheng LI[2], Wei-huan FANG[3]

(*1Marine Science School, Zhejiang Ocean University, Zhoushan 316000, China*)
(*2State Key Laboratory of Coastal and Offshore Engineering, Dalian University of Technology, Dalian 116024, China*)
(*3College of Animal Sciences, Zhejiang University, Hangzhou 310058, China*)
[†]E-mail: gui2237@163.com

**Abstract:** Numerical simulation and experimental tests were carried out to examine the hydrodynamic behaviors of a double-column floating system of gravity cage under wave conditions. A floating system of gravity cage can be treated as a small-sized floating structure when compared with the wavelengths. The main problem in calculating the wave loads on the small-sized floating structure is to obtain the reasonable force coefficients, which may differ from a submerged structure. In this paper, the floating system of gravity cage is simplified to a 2D problem, where the floating system is set symmetrically under wave conditions. The motion equations were deduced under wave conditions and a specific method was proposed to resolve the problem of wave forces acting on a small-sized floating system of gravity cage at water surface. Results of the numerical method were compared with those from model tests and the hydrodynamic coefficients $C_n$ and $C_\tau$ were studied. It is found that $C_n$ ranges from 0.6 to 1.0 while $C_\tau$ is between 0.4 and 0.6 in this study. The results are useful for research on the hydrodynamic behavior of the deep-water gravity sea cages.

**Key words:** Gravity cage, Floating system, Hydrodynamic coefficients, Waves
**doi:**10.1631/jzus.A0720016      **Document code:** A      **CLC number:** O353.2

## INTRODUCTION

The floating gravity cage aquaculture system is normally round or square with double floating pipes. Wave forces acting on it are complex, not only because its structure is complicated but also because it floats on the water surface, making the selection of correct hydrodynamic coefficients difficult. The Morison equation is used widely for cylinders with small size. However, the cylinders are usually below the water surface. Hydrodynamic coefficients of such structures have been studied extensively, using numerical and experimental methods, for both 2D and 3D flows. Miles and Gilbert (1968), Garrett (1971), Yeung (1981) and Sabuncu and Calisal (1981) had presented extensive data on hydrodynamic coefficients of vertical circular cylinders in water of limited depth. Numerous other floating structures of large size have also been studied. Sulisz and Johansson (1992) focused on the hydrodynamic coefficients of floating structures with rectangular profile. Feng (1996) presented a numerical method for calculating wave-induced loads on a pontoon within a time domain. Gou *et al.*(2004) studied the hydrodynamic interactions between waves and two connected floating structures through boundary integral equation method. Hamel (1992) and Li and He (1994) researched the hydrodynamic coefficients of rectangular cylinders under wave and wave-current flow conditions. As for structures like gravity sea cage floating system, Fredriksson *et al.*(2007) developed a

finite-element modeling method to determine its structural capabilities. However, they mainly focused on the static mechanics studies. Huang *et al.*(2006; 2007) discussed the hydrodynamics of a gravity-type cage under current and wave conditions. Values of the coefficients $C_n$ and $C_\tau$ used in computing wave and current loads on pipes are the same as those for a fully submerged circular cylinder. Although hydrodynamic coefficients of structures have been studied extensively, mostly they are focusing on either submerged or large-sized floating structures, but no effective method has been presented for evaluating the wave-induced forces and motion of small-sized floating structures. The major two problems encountered are: (1) the Morison equation is considered inapplicable for a structure floating on the water surface (Feng, 1996); (2) the wave-flow field around small floating structures is difficult to simulate.

In this paper, we deduced the motion equations under waves and proposed a special method for resolving the problem of wave forces acting on a floating system. In this way, the Morison equation is still applicable for studying hydrodynamic behavior of a small-sized floating structure. In addition, the hydrodynamic coefficients $C_n$, $C_\tau$ and $C_v$ are studied and suggestions for the selection of reasonable coefficient values in calculating wave forces on a double-column floating system are made. The results are valuable for research on the hydrodynamic behavior of the deep-water gravity sea cages.

## HYDRODYNAMIC FORCES ON FLOATING SYSTEM

The floating system of gravity cage is normally on the water surface, which makes the main parts for resisting the wave-induced loads. The floating system is simplified into a double-column pipe system, as shown in Fig.1. It is assumed that the floating system have no influence on waves since its size is much smaller compared to wavelength. The coordinate system is defined below as shown in Fig.1.

The floating system is divided into many micro-segments shown by a sketch in Fig.2. Two coordinate systems, *xyz* and *nτv*, are defined here since the floating system moves along with the waves. In the *xyz* coordinate system, the *x*-axis is along the wave

propagation direction and the *z*-axis is in the vertical direction. As for the *nτv* coordinate system, *n* and *τ* are in the normal and tangential directions of the micro-segment, respectively, and *v* is normal to the micro-segment plane *abcd*, as shown in Fig.2.
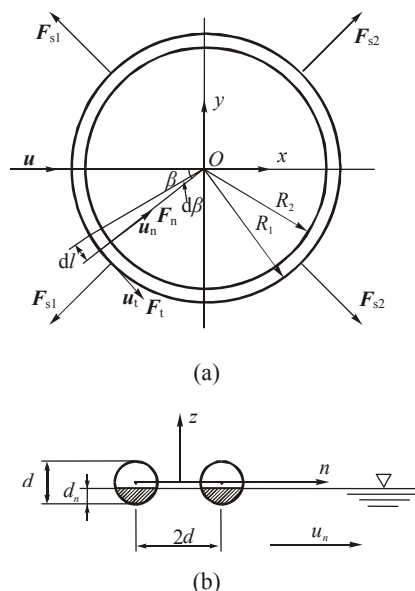


(a)

(b)

**Fig.1  Sketch of floating system of gravity cage. (a) Simplified floating system; (b) Section of double pipes**
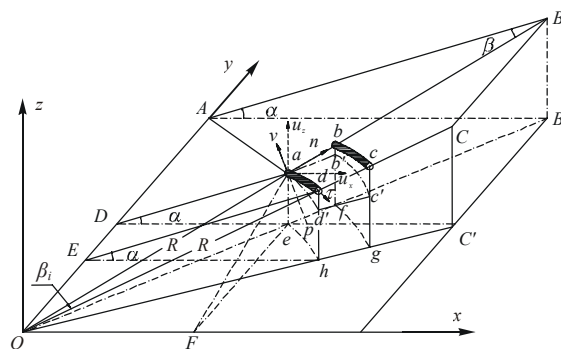


**Fig.2  Sketch of a micro-segment in calculating**

The floating system is simplified into 2D since it is set symmetrically in waves. It is easy to find that the inclination angle of the floating system varies within $[-2\pi, 2\pi]$. The wave particle velocities and accelerations are broken down into *x*- and *z*-axis components. As we have assumed that waves are not disturbed by the floating system, the velocities and accelerations of the wave particles can be calculated by the corresponding wave theory. In this paper, the third-order Stokes Wave Theory is introduced. The velocity and acceleration components are then broken

down into $n$ and $\tau$ directions within the $n\tau v$ coordinate system. We assume that the direction angles of the horizontal and vertical velocity components, $u_x$ and $u_z$, in $n\tau v$ are $\{\theta_n, \theta_\tau, \theta_v\}$ and $\{\omega_n, \omega_\tau, \omega_v\}$, respectively. Those angles have relationships with the inclination angle $\alpha$ of the floating system and the phase angle $\beta$ of the micro-segment plane (*abcd*), which should be calculated in advance. The relationships are easy to be obtained from Fig.2 as follows,

$$\begin{cases} \cos\theta_n = \cos\beta\cos\alpha, \\ \cos\theta_\tau = \sin\beta\cos\alpha, \\ \cos\theta_v = \sin\alpha. \end{cases} \quad (1)$$

**Wave forces**

The wave-induced hydrodynamic forces on each micro-segment can be calculated using the Morison equation. According to (Brebbia and Walker, 1979), the Morison equation includes two terms: the drag forces and the inertial forces in waves as shown in Eq.(2):

$$\boldsymbol{F} = C_D \rho A | \boldsymbol{u} - \boldsymbol{U} | \cdot (\boldsymbol{u} - \boldsymbol{U})/2 + \rho V_0 \boldsymbol{a} + C_m \rho V_0 (\boldsymbol{a} - \dot{\boldsymbol{U}}), \quad (2)$$

where $\boldsymbol{u}$ and $\boldsymbol{a}$ are the velocity and acceleration vectors of water particle respectively; $\boldsymbol{U}$ and $\dot{\boldsymbol{U}}$ are the velocity and acceleration vectors of water particle respectively; $\rho$ is water density; $V_0$ is the volume discharged by the micro-segment; $A$ is the projected area normal to the wave propagation direction; $C_D$ and $C_m$ are the drag and added mass coefficients, respectively.

1. Drag forces

The velocity components of wave particles in the $n\tau v$ coordinate system are obtained according to the direction angles given in Eq.(1), which are written as

$$\begin{cases} u_{xn} = u_x \cos\theta_n = u_x \cos\beta\cos\alpha, \\ u_{x\tau} = u_x \cos\theta_\tau = u_x \sin\beta\cos\alpha, \\ u_{xv} = u_x \cos\theta_v = -u_x \sin\alpha, \end{cases} \quad (3)$$

$$\begin{cases} u_{zn} = u_z \cos\omega_n = u_z \cos\beta\sin\alpha, \\ u_{z\tau} = u_z \cos\omega_\tau = u_z \sin\beta\sin\alpha, \\ u_{zv} = u_z \cos\omega_v = u_z \cos\alpha, \end{cases} \quad (4)$$

where $\{u_{xn}, u_{x\tau}, u_{xv}\}$ and $\{u_{zn}, u_{z\tau}, u_{zv}\}$ are the components of $u_x$ and $u_z$ in the $n\tau v$ coordinate system, respectively; $\alpha$ is the inclination angle of the floating system; $\beta$ is the phase angle of the micro-segment. Resultant velocities $\{u_n, u_\tau, u_v\}$ in the $n\tau v$ coordinate system are obtained as follows,

$$\begin{cases} u_n = u_{xn} + u_{zn} = u_x \cos\beta\cos\alpha + u_z \cos\beta\sin\alpha, \\ u_\tau = u_{x\tau} + u_{z\tau} = u_x \sin\beta\cos\alpha + u_z \sin\beta\sin\alpha, \\ u_v = u_{xv} + u_{zv} = -u_x \sin\alpha + u_z \cos\alpha. \end{cases} \quad (5)$$

Wave-induced drag forces on the micro-segment in the $n\tau v$ coordinate system can be obtained as follows by substituting Eq.(5) into the drag force term in Eq.(2).

$$\begin{aligned} F_n = C_n \rho A_n \, | (u_x - U_x)\cos\beta\cos\alpha + (u_z - U_z)\cos\beta\sin\alpha | \\ \cdot [(u_x - U_x)\cos\beta\cos\alpha + (u_z - U_z)\cos\beta\sin\alpha]/2, \end{aligned} \quad (6)$$

$$\begin{aligned} F_\tau = C_\tau \rho A_\tau \, | (u_x - U_x)\sin\beta\cos\alpha + (u_z - U_z)\sin\beta\sin\alpha | \\ \cdot [(u_x - U_x)\sin\beta\cos\alpha + (u_z - U_z)\sin\beta\sin\alpha]/2, \end{aligned} \quad (7)$$

$$\begin{aligned} F_v = C_v \rho A_v \, | -(u_x - U_x)\sin\alpha + (u_z - U_z)\cos\alpha | \\ \cdot [-(u_x - U_x)\cdot\sin\alpha + (u_z - U_z)\cos\alpha]/2, \end{aligned} \quad (8)$$

where $C_n$, $C_\tau$ and $C_v$ are the drag coefficients in the corresponding directions; $A_n$, $A_\tau$ and $A_v$ are the effective projected areas in the corresponding directions. Other parameters are the same as those described above. The values of the projected areas, $A_n$, $A_\tau$ and $A_v$, are different in the outer and inner pipes. They are related to the inclination angle $\alpha$ of the floating system, the phase angle $\beta$ of the micro-segment, the wave surface elevation and the gap between the outer and inner pipes. However, we neglect the difference since the gap between the outer and inner pipes is much smaller than the scale of the floating system and wavelength. Fig.3 is the model used in computing, where we assume that the outer and inner pipes are of the same profile. However, forces were doubled in calculating because there are two pipes.

According to Fig.3, it is assumed that $(x_i, y_i, z_i)$ are the central coordinates of the micro-segment. The depth under water of the micro-segment in $v$ direction is written as
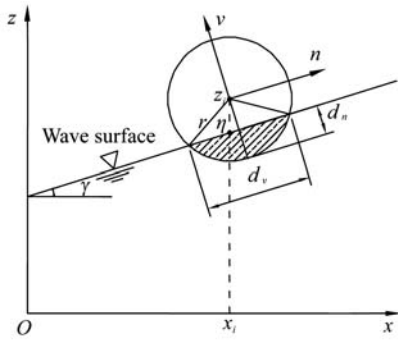
**Fig.3  Sketch of the simplified model in calculating**

$$d_n = r - (z_i - \eta) \cdot \cos\gamma, \tag{9}$$

where $\eta$ is the wave surface elevation, which can be calculated from the third-order Stokes Wave Theory; $r$ is the radius of the pipe; $\gamma$ is the inclination angle of wave profile at point $(x_i, y_i, z_i)$. The projected chord-length is obtained as

$$d_v = 2 \times \sqrt{r^2 - (r - d_n)^2} = 2 \times \sqrt{r^2 - (z_i - \eta)^2 \cdot \cos^2\gamma}. \tag{10}$$

The cross-section area under water is

$$S_i = (r^2 / 2)\phi_i - (r^2 / 2)\sin\phi_i, \tag{11}$$

where $\phi_i$ is the central angle against the projected chord-length, which is calculated by

$$\cos(\phi_i / 2) = 1 - d_n / r. \tag{12}$$

So far, the projected areas in different directions are as follows,

$$\begin{cases} A_n = d_n l_i = r l_i - (z_i - \eta) l_i \cos\gamma, \\ A_\tau = \dfrac{1}{\pi} r \phi_i l_i = \dfrac{2}{\pi} r l_i \arccos((z_i - \eta)\cos\gamma / r), \\ A_v = d_v l_i = 2 l_i \sqrt{r^2 - (z_i - \eta)^2 \cos^2\gamma}, \end{cases} \tag{13}$$

where $l_i$ is the length of the micro-segment. As for the projected area $A_\tau$ in the tangential direction, there are several methods for its calculation. Some take the cross-section projected area as $A_\tau$, which is often used for a short cylinder. Others take the product of cylinder diameter and length as $A_\tau$, which is usually introduced for a relative long cylinder, with the influence of the cross-section projected area on the tangential forces being small. In this paper, a new method is introduced since it is a floating system. The tangential forces may take an important role in the behavior of the floating system. $A_\tau$ is related to the arc area ($r\phi l_i$) of the micro-segment under water. When the micro-segment is fully submerged under water, the projected area $A_\tau$ should be the same as that calculated with the later method introduced above. Thus, the arc area of the micro-segment under water should be divided by a constant $\pi$, as shown in Eq.(13). For the normal projected area $A_v$, we let $d_v = 2r$ when $d_n \geq r$.

The motion equations of the floating system are established in the *xyz* coordinate system. Wave-induced drag forces should be transformed from the *nτv* coordinate system into the *xyz* coordinate system. The relationship is as follow,

$$\begin{bmatrix} F_{Dx} \\ F_{Dz} \end{bmatrix} = \begin{bmatrix} \cos\theta_n & \cos\theta_\tau & -\cos\theta_v \\ \cos\omega_n & \cos\omega_\tau & \cos\omega_v \end{bmatrix} \begin{bmatrix} F_n \\ F_\tau \\ F_v \end{bmatrix}. \tag{14}$$

By substituting corresponding variables into Eq.(14), the wave-induced drag forces acting on the micro-segment in the horizontal and vertical directions can be obtained. However, special processing of the wave-induced forces are necessary since the principle of wave action on floating pipes differs somewhat from fully submerged pipes. When calculating drag forces, we use the relative velocity between the wave particles and the pipe micro-segment. Drag forces would differ when the relative velocities are away from the pipe micro-segment since the floating pipe is on the surface with one side in water and the other in air. Thus, the vertical drag force component $F_v$ is modified by neglecting the normal force, i.e., having $F_v = 0$ under this circumstance since the upside of the micro-segment is exposed to air.

In Eqs.(6)~(8), the drag coefficients, $C_n$, $C_\tau$ and $C_v$, should be known in advance when calculating the wave-induced drag forces in the *nτv* coordinate system. They may differ from those of a circle cylinder fully submerged because they may be subject to the

effect of air-water surface tension. This paper is mainly focusing on the selection of reasonable values of those drag coefficients by using numerical simulation and experimental tests.

2. Inertial forces

According to (Brebbia and Walker, 1979), wave-induced inertial forces on a micro-segment can be written as

$$\begin{cases} F_{\mathrm{I}x} = \rho S_i l_i a_x + C_{\mathrm{m}x}\rho[(\pi \cdot d_n^{\,2})/4](a_x - \dot{U}_x), \\ F_{\mathrm{I}z} = \rho S_i l_i a_z + C_{\mathrm{m}z}\rho[(\pi \cdot d_v^{\,2})/4](a_z - \dot{U}_z), \end{cases} \quad (15)$$

where $F_{\mathrm{I}x}$ and $F_{\mathrm{I}z}$ are the inertial forces in $x$ and $z$ directions, respectively; $a_x$ and $a_z$ are the acceleration components in $x$ and $z$ directions, respectively; $\dot{U}_x$ and $\dot{U}_z$ are the acceleration components of the micro-segment in $x$ and $z$ directions, respectively. $C_{\mathrm{m}x}$ and $C_{\mathrm{m}z}$ are the added mass coefficients in $x$ and $z$ directions, respectively, whose values are discrete under wave conditions, and depend on both $Re$ and $KC$ numbers; their average values under various wave conditions are 0.2~1.0, as described by Li (1989). In this paper, for simplicity, we take the added mass coefficients as constant: $C_{\mathrm{m}x}=C_{\mathrm{m}z}=0.2$.

**Buoyancy and mooring-line forces**

Gravity of the micro-segment is written as

$$G_i = G / N, \quad (16)$$

where $G$ is the total gravity of the floating system; $N$ is the number of the micro-segments. According to Fig.3, the buoyancy acting on a micro-segment is calculated by

$$F_{\mathrm{f}i} = \rho g S_i l_i = \rho g (r^2 / 2)(\phi_i - \sin\phi_i)l_i. \quad (17)$$

Mooring-line forces are relative to the displacement of the fore and back cleat points on the floating system. Displacements of the cleat points are obtained by calculating their dynamic coordinates. The relationship between the elongation and mooring-line forces is obtained through experimental measurements, which is written as

$$F_{\mathrm{s}} = -343.83(\Delta S / S)^2 + 79.14\Delta S / S, \quad (18)$$

where $\Delta S$ is the elongation of the mooring-line (m); $S$ is the original length of the mooring-line (m); $F_{\mathrm{s}}$ is the tension in the mooring-line (N).

MOTION EQUATIONS

Forces on the whole floating system are obtained by evaluating the forces on the micro-segments, as described previously. In general, the relative movement of each micro-segment is confined in a very small range of displacement; otherwise, breakage could occur and the structure's integrity would be destroyed. Thus we treated the floating system as a rigid body, and the micro-segment were restrained by rigid body motion. In general, a rigid body motion involves six degrees of freedom including three translational and three rotational motions. In this paper, our discussion is limited to a 2D field because the floating system is set symmetrically to waves. Thus, the rigid body motion is simplified into three degrees of freedom including two translational and one rotational motions. Following (Jia, 1987), two translation equations derived from Newton's second law and one rotation equation (known as Euler's equation of motion) are written as follows,

$$\begin{cases} \ddot{x} = -\dot{z}\dot{\phi} + (1/m)\sum_{i=1}^{N} F_{xi}, \\ \ddot{z} = \dot{x}\dot{\phi} + (1/m)\sum_{i=1}^{N} F_{zi}, \\ \ddot{\phi} = (1/I)\sum_{i=1}^{N} M_i, \end{cases} \quad (19)$$

where $F_{xi}$ is the force in $x$ direction at the $i$th micro-segment; $N$ is the number of total micro-segments; $m$ is the total mass of the floating system; $M_i$ is the moment at the $i$th micro-segment; $\phi$ is the rotation angle of the floating system; and $I$ is the principal moment of inertia of the floating system defined as

$$I = mR^2 / 2, \quad (20)$$

where $R$ is the radius of the floating system.

The motion Eq.(19) is a group of second-order differential equations and can be calculated with a numerical method, such as Runge-Kutta method. For

a second-order differential equation,

$$\ddot{\boldsymbol{\xi}} = \boldsymbol{F}(\Delta t, \boldsymbol{\xi}, \dot{\boldsymbol{\xi}}). \qquad (21)$$

Displacement and velocity of a moving object can be written as follows when calculated with the fourth-order Runge-Kutta method,

$$\boldsymbol{\xi}(t+\Delta t) = \boldsymbol{\xi}(t) + \Delta t\dot{\boldsymbol{\xi}}(t) + \Delta t(K_1 + K_2 + K_3)/6, \quad (22)$$

$$\dot{\boldsymbol{\xi}}(t+\Delta t) = \dot{\boldsymbol{\xi}}(t) + (K_1 + 2K_2 + 2K_3 + K_4)/6, \qquad (23)$$

and

$$K_1 = \Delta t \boldsymbol{F}(t, \boldsymbol{\xi}(t), \dot{\boldsymbol{\xi}}(t)),$$

$$K_2 = \Delta t \boldsymbol{F}(t+\Delta t/2, \boldsymbol{\xi}(t) + \Delta t\dot{\boldsymbol{\xi}}(t)/2, \dot{\boldsymbol{\xi}}(t) + K_1/2),$$

$$K_3 = \Delta t \boldsymbol{F}(t+\Delta t/2, \boldsymbol{\xi}(t)+\Delta t\dot{\boldsymbol{\xi}}(t)/2+\Delta tK_1/2, \dot{\boldsymbol{\xi}}(t)+K_2/2),$$

$$K_4 = \Delta t \boldsymbol{F}(t+\Delta t, \boldsymbol{\xi}(t) + \Delta t\dot{\boldsymbol{\xi}}(t) + \Delta tK_2/2, \dot{\boldsymbol{\xi}}(t) + K_3).$$

During calculation, the gravity, buoyancy, wave and mooring-line forces are determined according to the displacement $\boldsymbol{\xi}(t)$ and velocity $\dot{\boldsymbol{\xi}}(t)$ at time $t$. Then, acceleration $\ddot{\boldsymbol{\xi}}(t)$ can be obtained by Eq.(21). Displacement $\boldsymbol{\xi}(t+\Delta t)$ and velocity $\dot{\boldsymbol{\xi}}(t+\Delta t)$ at time $(t+\Delta t)$ can be determined through Eqs.(22) and (23). The calculating process is repeated until the end of the designated time.

NUMERICAL RESULTS AND EXPERIMENTAL DATA

Model tests of a simplified floating system were carried out to compare with the simulation results. The model was assembled in the middle of the wave-current flume tank at the State Key Laboratory of Coastal and Offshore Engineering of Dalian University of Technology. The wave-current flume tank is 69 m long, 2 m wide and 1.8 m high, equipped with a regular wave-maker and current-producing system. The model set-up is shown in Fig.4a. Parameters of the model in detail are given in Table 1. The mooring-line forces were measured by four transducers attached to the bottom of each mooring-line. One diode was fixed on the middle of the floating system for motion analysis. A serial of 8-bit format images were captured through a Charge Coupled Device (CCD) camera set aside the flume tank, as shown in Fig.4b. Special software with an accuracy of 6% was

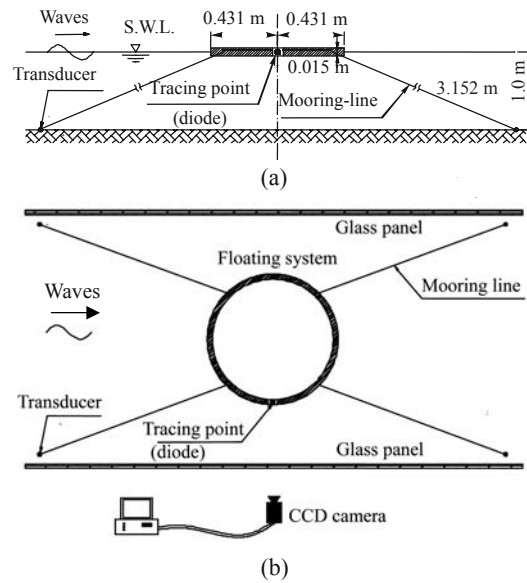developed for tracing the diode under wave conditions (Fig.5).



**Fig.4 Sketch of the simplified floating system in waves**
(a) Side view; (b) Top view

**Table 1 Parameters of the simplified floating system**

| | Parameter | Value |
|---|---|---|
| Outer circle | General diameter (m) | 0.846 |
| | Pipe diameter (m) | 0.0153 |
| | Material | HDPE[*] |
| Inner circle | General diameter (m) | 0.796 |
| | Pipe diameter (m) | 0.0153 |
| | Material | HDPE[*] |
| Mooring-line | Length (m) | 3.152 |
| | Diameter (m) | 0.0012 |
| | Material | PE[**] |

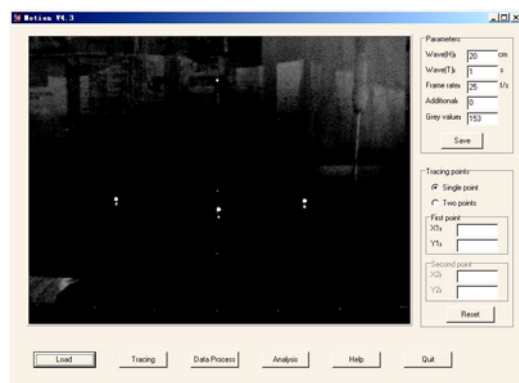[*] HDPE: High-density polyethylene; [**] PE: polyethylene



**Fig.5 Software for analyzing the dynamic images obtained via a CCD camera**

As described previously, the coefficients $C_n$, $C_\tau$ and $C_v$ need to be determined in advance for numerical calculation. For the coefficients $C_n$ and $C_v$, the velocity components in $n$ and $\tau$ directions are normal to the axes of the micro-segment. For simplicity, we assume that they are of the same values, i.e., $C_n=C_v$. Based on this assumption, only the coefficients $C_n$ and $C_\tau$ are left undetermined. In this paper, the reasonable values of the two coefficients were discussed based on the results through numerical simulation and model tests. The maximum values of mooring-line forces, horizontal and vertical displacements are selected for comparisons. The numerical results with different values for coefficients $C_n$ and $C_\tau$ are compared with the experimental data, as shown in Figs.6 and 7.

As shown in Fig.6, taken the tangent coefficient as a constant ($C_\tau=0.6$), the maximum values of the mooring-line forces and the horizontal displacements increase with the increase of the normal coefficient. However, the changes of vertical displacements seem small. In the same way, when taking the normal coefficient as a constant ($C_n=0.8$), we have the similar results to those discussed above, as shown in Fig.7. In addition, coefficients may have certain relationship with wave parameters. However, it is a complex problem because there are many factors involved, which need more works in the future.
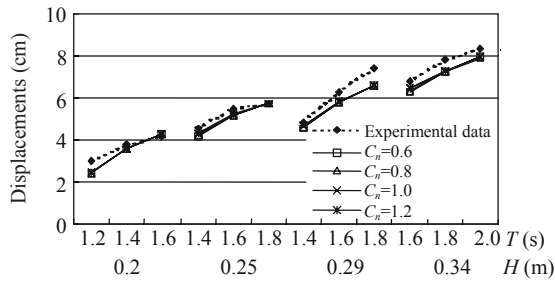
This paper aims to find the reasonable values for these coefficients. The standard deviation method is introduced, as shown in Eq.(24):
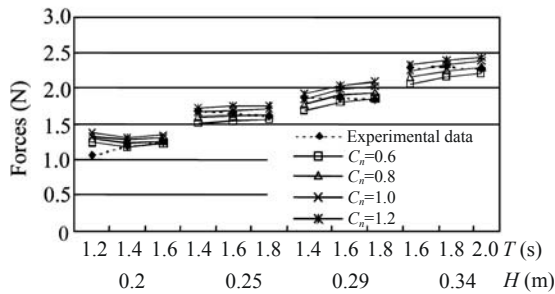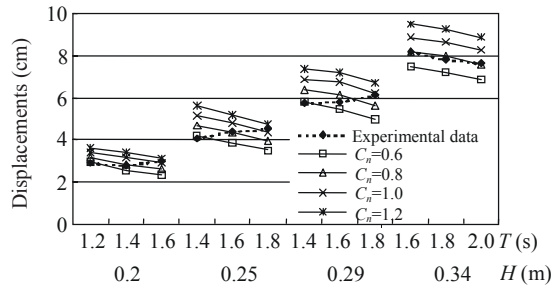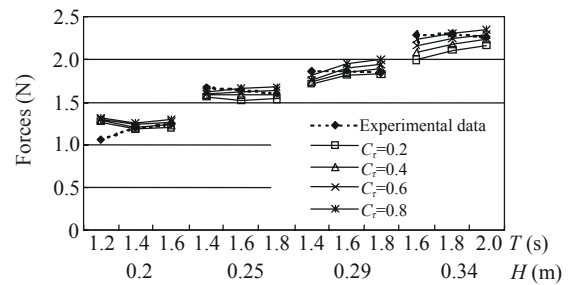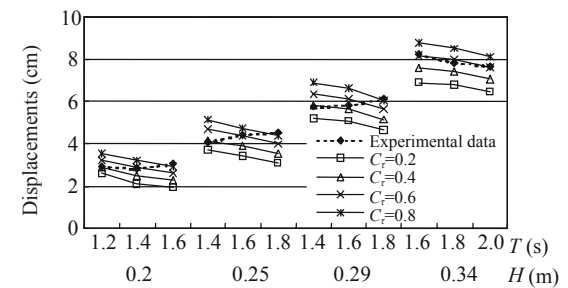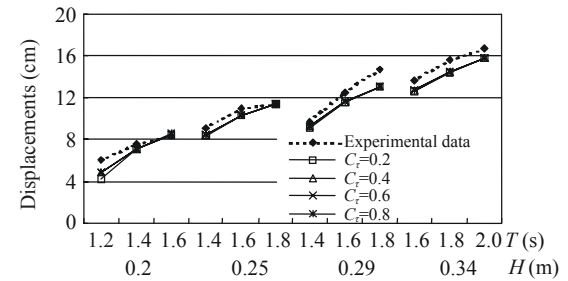


**Fig.6  Mooring-line forces (a), vertical displacement (b), horizontal displacement (c) comparison of numerical vs experimental data ($C_\tau=0.6$ as constant)**



**Fig.7  Mooring-line forces (a), vertical displacement (b), horizontal displacement (c) comparison of numerical vs experimental data ($C_n=0.8$ as constant)**

$$\sigma = \sqrt{\frac{1}{(n-1)} \sum_{i=1}^{n} (F_{ci} - F_{ei})^2}, \qquad (24)$$

where $n$ is the sample number that refers to the number of waves with different heights and periods. In this paper, $n$ equals 12. $F_{ci}$ and $F_{ei}$ denote the calculated results and experimental data, respectively. The square errors calculated are listed in Table 2.

As shown in Table 2, the mooring-line forces and the horizontal displacements are of minimum values for $C_\tau$=0.6 and $C_n$=0.8. For the vertical displacements, the least square error decreases as coefficients increase. However, the coefficients seem to have a relatively small effect on the vertical displacements, as inferred from Table 2. Thus, we take the mooring-line forces and the horizontal displacements as reference for selection of reasonable values of drag coefficients under wave conditions. In this paper, we suggest (0.4~0.8) for the tangential coefficient and (0.6~1.0) for the normal coefficients. It is found that the values for normal coefficients are within the widely used range for fully submerged circle cylinders (Li, 1989). However, the values for tangential coefficients are much bigger than those for fully submerged circular cylinders whose values mainly vary from 0.02 to 0.1 (Wang, 1995; Takagi *et al.*, 2002; 2004).

More comparisons of the horizontal and vertical displacements in time-series are given in Figs.8 and 9, in which, the solid lines denote the numerical results and the dots denote the experimental data.

As shown in Figs.8 and 9, the positive parts of horizontal displacements of the numerical results agree well with the experimental data. However, errors appear at the lower parts. The reasons for the results are complex, one of which is that the floating system is made of flexible HDPE pipes whose suppleness is not considered in this paper as we simplify the floating system into a rigid body to avoid difficulties in calculating motion equations. When the floating system stays at the trough of waves, some parts of the pipes, which are below the water surface during the experimental tests, are above the water surface during the numerical simulations. As described previously, the tangential drag forces are significantly attributed to the hydrodynamic behavior but the effects are weakened during the numerical simulations. When the floating system stays at the crest of waves, the influence of the pipe suppleness on the results is much smaller since the area and the volume of the pipe under water have no obvious changes. In addition, coefficients were treated as constants during simulations. However, the area and volume under water of each micro-segment differs from each other. This may also account for the errors raised.

CONCLUSION

This paper focused on the evaluation of the hydrodynamic behavior of a floating system. The determinations of the hydrodynamic coefficients $C_n$ and $C_\tau$ are the main points discussed. Numerical

**Table 2  The square errors calculated with Eq.(24)**

| Item | $C_t$ | $C_n$ | Square error | Item | $C_t$ | $C_n$ | Square error |
|---|---|---|---|---|---|---|---|
| Mooring-line forces | 0.6 | 0.6 | 0.131 | Mooring-line forces | 0.2 | 0.8 | 0.151 |
| | 0.6 | 0.8 | 0.100 | | 0.4 | 0.8 | 0.117 |
| | 0.6 | 1.0 | 0.120 | | 0.6 | 0.8 | 0.100 |
| | 0.6 | 1.2 | 0.162 | | 0.8 | 0.8 | 0.106 |
| Horizontal displacements | 0.6 | 0.6 | 0.667 | Horizontal displacements | 0.2 | 0.8 | 1.055 |
| | 0.6 | 0.8 | 0.395 | | 0.4 | 0.8 | 0.595 |
| | 0.6 | 1.0 | 0.698 | | 0.6 | 0.8 | 0.395 |
| | 0.6 | 1.2 | 1.129 | | 0.8 | 0.8 | 0.662 |
| Vertical displacements | 0.6 | 0.6 | 0.930 | Vertical displacements | 0.2 | 0.8 | 1.016 |
| | 0.6 | 0.8 | 0.898 | | 0.4 | 0.8 | 0.914 |
| | 0.6 | 1.0 | 0.860 | | 0.6 | 0.8 | 0.898 |
| | 0.6 | 1.2 | 0.826 | | 0.8 | 0.8 | 0.883 |
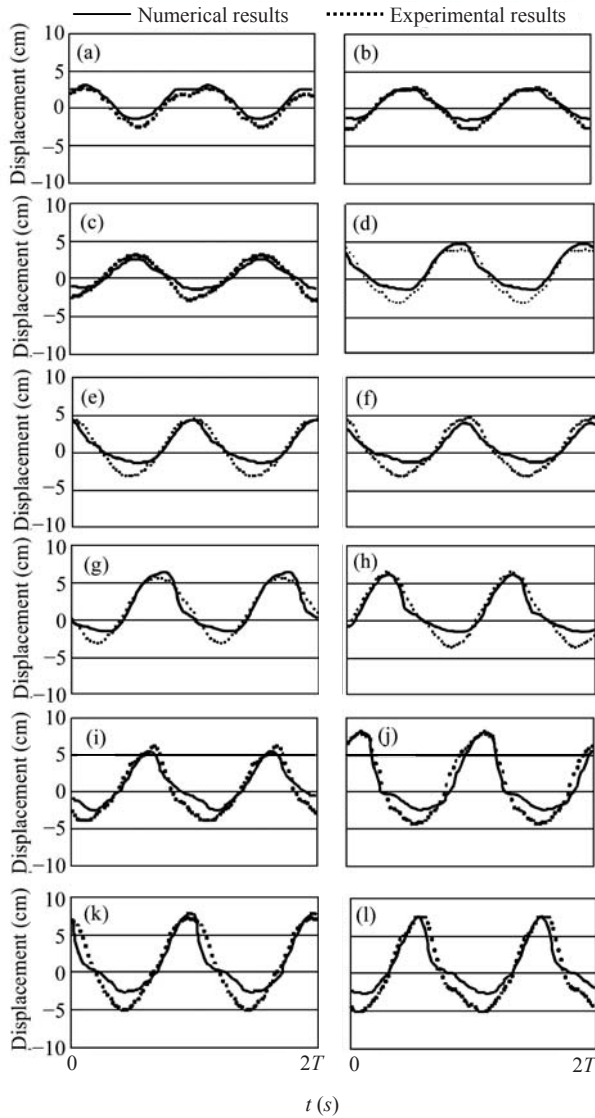
**Fig.8  Horizontal displacement: comparison of numerical vs experimental data**
(a) *H*=20 cm, *T*=1.2 s; (b) *H*=20 cm, *T*=1.4 s; (c) *H*=20 cm, *T*=1.6 s; (d) *H*=25 cm, *T*=1.4 s; (e) *H*=25 cm, *T*=1.6 s; (f) *H*=25 cm, *T*=1.8 s; (g) *H*=29 cm, *T*=1.4 s; (h) *H*=29 cm, *T*=1.6 s; (i) *H*=29 cm, *T*=1.8 s; (j) *H*=34 cm, *T*=1.6 s; (k) *H*=34 cm, *T*=1.8 s; (l) *H*=34 cm, *T*=2.0 s

**Fig.9  Vertical displacement comparison of numerical vs experimental data**
(a) *H*=20 cm, *T*=1.2 s; (b) *H*=20 cm, *T*=1.4 s; (c) *H*=20 cm, *T*=1.6 s; (d) *H*=25 cm, *T*=1.4 s; (e) *H*=25 cm, *T*=1.6 s; (f) *H*=25 cm, *T*=1.8 s; (g) *H*=29 cm, *T*=1.4 s; (h) *H*=29 cm, *T*=1.6 s; (i) *H*=29 cm, *T*=1.8 s; (j) *H*=34 cm, *T*=1.6 s; (k) *H*=34 cm, *T*=1.8 s; (l) *H*=34 cm, *T*=2.0 s

results show that the tangential coefficient $C_\tau$ (0.4~0.8) for a pipe in waves is much larger than that of a fully submerged circular cylinder, which is mainly within (0.02~0.1) as described by the former research (Wang, 1995; Takagi *et al.*, 2002; 2004). The effects of the surface tension may account for the difference. For normal coefficient $C_n$ (0.6~1.0), its value is within the commonly used range described by Li (1989) and Hou and Gao (1998). In addition, coefficients may have certain relationship with wave parameters. However, it is a complex problem due to
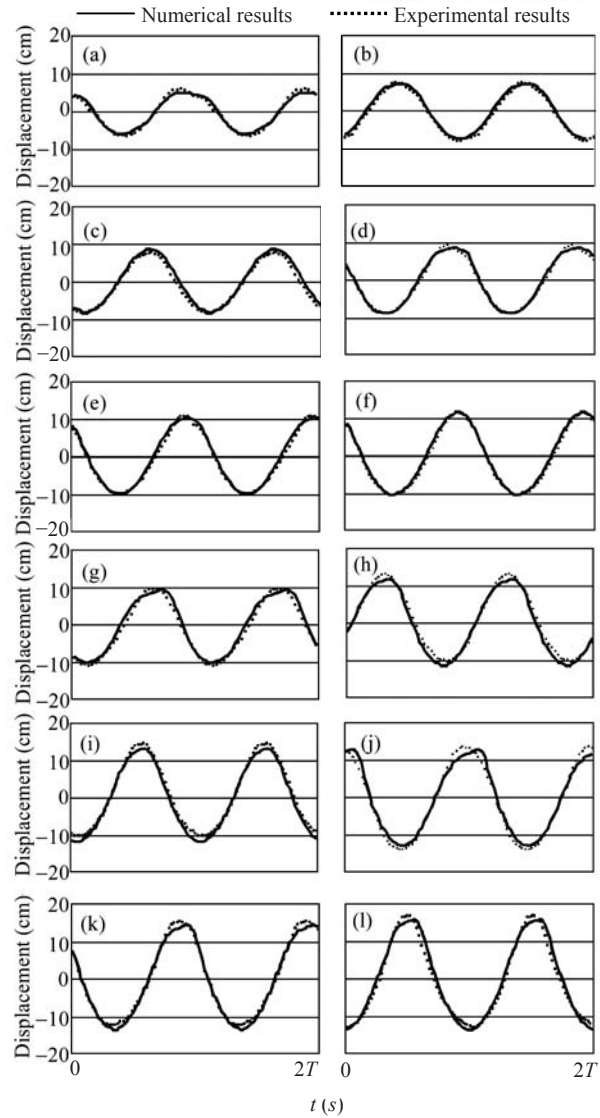
many factors involved, which need more works in the future. Studies on the hydrodynamic coefficients of a floating system under wave conditions will enhance further research on the behavior of sea cages in open sea.

**References**

Brebbia, C.A., Walker, S., 1979. Dynamic Analysis of Offshore Structure. Newnes-Butterworths, London, England, p.109-143.

Feng, T.C., 1996. Wave exciting forces on floats. *Ocean Engineering*, **14**(3):36-40 (in Chinese).

Fredriksson, D.W., Decew, J.C., Tsukrov, I., 2007. Development of structural modeling techniques for evaluating HDPE plastic net pens used in marine aquaculture. *Ocean Engineering*, **34**(16):2124-2137. [doi:10.1016/j.oceaneng.2007.04.007]

Garrett, C.J.R., 1971. Wave forces on a circular dock. *Journal of Fluid Mechanics*, **46**(1):129-139. [doi:10.1017/S0022112071000430]

Gou, Y., Teng, B., Ning, D.Z., 2004. Interaction effects between wave and two connected floating bodies. *Engineering Science*, **6**(7):75-80 (in Chinese).

Hamel, D.D., 1992. Forces on vertical rectangular cylinder in wavy flow and in combined wave and current flow at low KC number. *OMAE A*, (1992):293-298.

Hou, E.H., Gao, Q.L., 1998. Theory and Design of Fishing Gear. The Ocean Press, Beijing, China, p.41-47 (in Chinese).

Huang, C.C., Tang, H.J., Liu, J.Y., 2006. Dynamical analysis of net cage structures for marine aquaculture: Numerical simulation and model testing. *Aquacultural Engineering*, **35**(3):258-270. [doi:10.1016/j.aquaeng.2006.03.003]

Huang, C.C., Tang, H.J., Liu, J.Y., 2007. Modeling volume deformation in gravity-type cages with distributed bottom weights or a rigid tube-sinker. *Aquacultural Engineering*, **37**(2):144-157. [doi:10.1016/j.aquaeng.2007.04.003]

Jia, S.H., 1987. Rigid Body Dynamics. Higher Education Press, Beijing, China, p.153-157 (in Chinese).

Li, Y.C., 1989. Wave Action on Maritime Structures. The Press of Dalian University of Technology, Dalian, China, p.144-145.

Li, Y.C., He, M., 1994. Forces on rectangular cylinder of small size in combined wave and current flow. *China Offshore Platform*, **9**(Z1):293-298 (in Chinese).

Miles, J., Gilbert, F., 1968. Scattering of gravity waves by a circular dock. *Journal of Fluid Mechanics*, **34**(4):783-793. [doi:10.1017/S0022112068002235]

Sabuncu, T., Calisal, S., 1981. Hydrodynamic coefficients for vertical circular cylinders at finite depth. *Ocean Engineering*, **8**(1):25-63. [doi:10.1016/0029-8018(81)90004-4]

Sulisz, W., Johansson, M., 1992. Second order wave loading on a horizontal rectangular cylinder of substantial draught. *Applied Ocean Research*, **14**(6):333-340. [doi:10.1016/0141-1187(92)90038-L]

Takagi, T., Suzuki, K., Hiraishi, T., 2002. Development of the numerical simulation method of dynamic fishing net shape. *Nippon Suisan Gakkaishi*, **68**(3):320-326.

Takagi, T., Shimizu, T., Suzuki, K., Hiraishi, T., Yamamoto, K., 2004. Validity and layout of "NaLA": a net configuration and loading analysis system. *Fisheries Research*, **66**(2-3):235-243. [doi:10.1016/S0165-7836(03)00204-2]

Wang, E.G., 1995. Mechanics of Fishing Gear. Dalian Fisheries University, Dalian, China, p.33-36 (in Chinese).

Yeung, R.W., 1981. Added mass and damping of a vertical cylinder in finite-depth waters. *Applied Ocean Research*, **3**(3):119-133. [doi:10.1016/0141-1187(81)90101-2]